Highthroughput fabrication of carbonized electrospun polyacrylonitrile/poly(acrylic acid) nanofibers with additives for enhanced electrochemical sensing

Received: 10 December 2019 | Revised: 6 March 2020 | Accepted: 3 April 2020

DOI: 10.1002/app.49341

ARTICLE

Journal of Applied Polymer Science WILEY

High-throughput fabrication of carbonized electrospun polyacrylonitrile/poly(acrylic acid) nanofibers with additives for enhanced electrochemical sensing

Huey Ling Tan[1] | **Maria Kana Sanira Putri**[2] | **Siti Shawalliah Idris**[1] | **Niklas Hartikainen**[2] | **Noor Fitrah Abu Bakar**[1] | **Antonios Keirouz**[2] | **Norbert Radacsi**[2]

[1]Faculty of Chemical Engineering, Universiti Teknologi MARA, Shah Alam, Selangor, Malaysia

[2]School of Engineering, Institute for Materials and Processes, The University of Edinburgh, King's Buildings, Edinburgh, UK

Correspondence
Huey Ling Tan, Faculty of Chemical Engineering, Universiti Teknologi MARA, 40450 Shah Alam, Selangor, Malaysia.
Email: hueyling@uitm.edu.my

Norbert Radacsi, School of Engineering, Institute for Materials and Processes, The University of Edinburgh, King's Buildings, Edinburgh, EH9 3FB, UK.
Email: n.radacsi@ed.ac.uk

Funding information
The University of Edinburgh, Grant/Award Number: 100-IRMI/INT 16/6/2 (010/2017); Universiti Teknologi MARA; University of Edinburgh

Abstract

Lightweight, polyacrylonitrile-derived electrodes with different additives were fabricated using high-throughput nozzle-free electrospinning. The electrospun precursor nanofibers (PNFs) containing iron oxide, gold nanoparticles, or reduced graphene oxide (rGO) were subjected to oxidative stabilization and carbonization to obtain a carbon-rich conductive nanofiber structure. Scanning electron microscopy showed that the carbon nanofibers contracted between 11 and 55% while the Fourier-transform infrared spectroscopy confirmed that the carbon nanofibers were thermally stable. Thermogravimetric and differential scanning calorimetry results revealed that the cross-linking of the chain molecules and cyclization were completed. Next, cyclic voltammetry results indicated that the electroactivity of the modified screen-printed carbon electrodes was decreased by 85% due to the presence of carbon glue. The modified device presented significant enhanced electrochemical responses with the inclusions of nanoparticles, with rGO showing a 2.13 times higher electroactive surface area, followed by iron oxide (two times) and gold nanoparticles (1.37 times) than the equivalent PNFs.

KEYWORDS

cyclic voltammetry, degradation, electroactive surface area, nanoparticles, nozzle-free electrospinning

1 | INTRODUCTION

The development of analytical methods and platforms that are sensitive, affordable and easy to use, is of utmost importance for the effective sensing of analytes. Nanofibers (NFs) have attracted great attention due to

Abbreviations: AuNPs, gold nanoparticles; CNFs, carbon nanofibers; CV, cyclic voltammetry; GO, graphene oxide; IO, iron (III) oxide; NFs, nanofibers; PAA, Polyacrylic acid; PAN, polyacrylonitrile; PNFs, precursor nanofibers; rGO, reduced graphene oxide; SPCE, screen-printed carbon electrode.

their unique structural and physical properties; such as small fiber diameters, large surface area per unit mass, small pore size, increased porosity and flexibility in surface functionalization.[1–4] Many different strategies have been developed for their synthesis and production, with electrospinning being the most versatile, straightforward, and cost-effective technique when comparing to others, such as template synthesis,[5] phase separation and self-assembly.[6] NFs produced by electrospinning have many unique characteristics, such as high surface-to-mass (or volume) ratio, ability to form highly porous fibrous membranes with excellent pore interconnectivity, controllability in fiber diameter, surface morphology and fibrous structure.[7–9]. NFs are also easy to be functionalized during the electrospinning process using metal oxides or nanoparticles, such as nickel oxide, titanium oxide, iron oxide, gold nanoparticles, and reduced graphene oxide (GO) to produce nanofibers with high tensile strength, large surface area, enhanced electrical and catalytic properties.[10–12] Unlike the conventional needle-based electrospinning, nozzle-free electrospinning can be used for large-scale production of nanofibers.[13] These unique features have provided electrospun NFs with enormous opportunities to be used in various fields including tissue engineering scaffolds, filtration, sensors, and energy storage, affinity membranes and many others.[14–16]

Electrospun NFs have subsequently been introduced as electrode materials finding applications in energy storage, such as lithium-ion batteries due to their high specific surface area.[17–19] Various polymeric materials have been used as backbone polymers, with polyacrylonitrile (PAN) being the most suitable precursor compared to pitch- or cellulose-based precursor.[20,21] Carbonization of the PAN-based NFs can produce high-performance carbon fibers with greater carbon yield (>50% of the original precursor mass).[22] Other advantages include improved mechanical and electrical properties,[23] wide potential windows, relatively inert electrochemistry, low cost and good electrocatalytic activity for many redox reactions.[24,25] These properties can be further controlled by heat treatment cycles during stabilization and carbonization. Polyacrylic acid (PAA) is a highly water-soluble anionic polyelectrolyte due to its charged carboxyl side chains.[6,7,12] PAA can improve the processability of acrylonitrile while decreasing the cyclization temperature.[23,26] The negatively charged active site of PAA is also ideal for cation loading to fabricate highly conductive films.[10,11,27]

It is important to evaluate the intrinsic electrochemical properties of carbon nanofibers (CNFs) to explore their full potential in sensing applications. However, CNF-based sheets after heat treatment are extremely fragile and lightweight, rendering the preparation and evaluation of the CNFs as working electrodes very challenging without altering its physical conditions and additional re-treatment. The as-prepared CNFs are normally ground and dispersed with auxiliary additives (such as carbon black and binders), which afterward are layered or coated with reinforced fibers or metal during the electrode fabrication process.[28–30] However, grinding the carbonized nanofibers destroys the nanostructure, and the presence of the additives and reinforcing materials may lead to undesired chemical reactions[31–33]; hence, the real sensing capability of the CNFs alone is not assessable.

In this work, the nozzle-free electrospinning method was used to fabricate precursor nanofibers (PNFs) from PAN and co-polymer PAA. PAA acted as a sacrificial polymer allowing the formation of porous CNFs upon the removal of PAA by heat treatment. Nanoparticles of gold (AuNPs), iron oxide (IO), or GO were added to the polymeric solutions during the electrospinning process to enhance the electrical properties of the NFs.[27] Subsequently, PNFs or CNFs containing AuNPs, IO, or rGO were attached to a commercially available screen-printed carbon electrode (SPCE) using a conductive glue without any alteration to the physical conditions. The influence of the conductive glue to the overall electronic conductivity was evaluated and used as the baseline to compare the analytical performance of the modified SPCEs containing different nanoparticles. All of the modified SPCEs were tested in the presence of hydrogen peroxide (H_2O_2) or ferri/ferro cyanide ($Fe[CN]_6^{3-/4-}$) to evaluate their analytical performance. The performance of the SPCEs modified with different CNFs was evaluated and compared to PNFs.

2 | MATERIALS AND METHODS

2.1 | Materials

Polyacrylonitrile (PAN, Mw 150,000 g mol^{-1}) and poly(acrylic acid) (PAA, Mw 450,000 g mol^{-1}) were purchased from Shandong Jianofu Treasure Industrial Co. Ltd (China) and Sigma-Aldrich (USA), respectively. *N*,*N*-dimethylformamide 99% (DMF) was purchased from Alfa-Aesar (USA). Gold nanoparticles (AuNPs, average particle size 40 nm) in an aqueous solution were vacuumed dried and added to the electrospinning polymer solution. Alternatively, 0.4 g mL^{-1} of iron(III) oxide solid particles (IO, average size <60 μm) were added to the electrospinning solution. GO (average size <25 μm) was synthesized by the modified Tour's method.[34] Potassium ferricyanide ($K_3Fe[CN]_6$), hydrogen peroxide (H_2O_2), sodium phosphate buffer saline (PBS), potassium

chloride (KCl) and all other reagents were purchased from Sigma-Aldrich (USA). 1 mM $K_3[Fe(CN)_6]$ was used as a redox probe couple. The screen-printed carbon electrodes (Metrohm Dropsens, DRP C110) purchased from Metrohm (Switzerland) had carbon working (diameter: 4 mm) and counter electrodes, and Ag as the reference electrode. PELCO® conductive carbon glue was used to attach the nanofibers to the SPCE.

2.2 | GO synthesis, purification, and exfoliation

Modified Tour's method[29] was used to synthesize the graphene oxide (GO). Briefly, acids mixture of sulfuric acid and phosphoric acid was slowly mixed into the solid mixture consisting of graphite and potassium permanganate, the reaction temperature was controlled to below 50°C. The solution was stirred in a round bottom flask placed in a water bath at 50°C for 12 hours. The reaction mixture was then allowed to cool to room temperature overnight. Next, the reaction mixture was slowly poured into a beaker with cold water on an ice bath, with controlled temperature not more than 27°C. H_2O_2 was then slowly added to the solution until color changed from dark purple to light brown. Next, the reaction products were centrifuged at 4,000 rpm 10 minutes for 10 times and the heavier phase was collected and diluted in ultrapure water between each run. The products of the centrifuging were dialyzed in ultrapure water. Purified GO was exfoliated through sonication for 4 hr with sonication power of 150 W. The GO was separated using centrifugation at 4,000 rpm for 10 minutes before powdering it.

2.3 | Electrospinning of PAA/PAN fibers

Initially, 12 wt% PAA in DMF was dissolved overnight at 150°C/700 rpm. Then, 12 wt% PAN was dissolved in DMF and stirred at 700 rpm for 3 hr at 80°C. The two prepared solutions were then mixed at a 7:1 PAN:PAA w/w ratio and stirred at 180°C for 15–20 min, to prepare the master solution. Additive solutions were prepared separately before being added to the master solution (Tables 1 and 2). To prepare NFs decorated with AuNPs, 15.5 nM of AuNPs in DMF was added to the master solution, which resulted in 93:7 v/v ratio of (PAN/PAA): AuNP suspension and the mixture was stirred at 45°C for 10 min before electrospinning. NFs containing IO were prepared by adding iron(III) oxide to the master solution, resulting in 97:3 v/w ratio of (PAN/PAA):IO. The suspension was stirred overnight at 100°C and sonicated for 1 hr before electrospinning to increase the dispersion of the IO particles in the suspension. PNFs decorated with GO were prepared by sonicating 3 wt% of GO in DMF for overnight before adding to the polymer mixture for electrospinning. While CNFs incorporated with GO were prepared by vacuum coating 1 mg mL^{-1} GO solution on the electrospun nanofibers using a vacuum filtration apparatus. The excess GO was rinsed in a bath of ultrapure water while gently agitating the nanofibers in the water. The nanofibers and GO were then calcined and reduced simultaneously in a furnace (heating at 650°C for 2 hr with a heating rate of 5°C min^{-1} in hydrogen atmosphere).

A nozzle-free electrospinning device was used to allow the inclusion of additive particles in the polymer without the problem of nozzle clogging. The electrospinning apparatus consisted of a motorized rotating solid stainless-steel electrode (electrospinning electrode) inside a Teflon bath, where the different solutions or suspensions were poured. Using a DeWalt (model D26411) 1,800 W heat gun, the collector electrode was under constant hot airflow of 450 L min^{-1} at a temperature of 150°C throughout the electrospinning process. The distance between the electrospinning electrode and collector electrode (working distance) was 15 cm. A potential difference of 60 kV DC was applied between two rotating electrodes (+30 kV on the electrospinning electrode inside the pool and − 30 kV on the collector electrode). A cellulose-based paper (commercial baking paper) was used to collect the fibers. All experiments were carried out under ambient conditions at a relative

TABLE 1 Summary of the electrospinning polymer solutions and blending ratios

Polymer blend	Ratio (PAN: PAA) (w/w)
12% PAN (w/v) (M_w = 150,000 g mol^{-1}) + 12% PAA (w/v) (M_w = 450,000 g mol^{-1})	7:1

Abbreviation: PAN/PAA, polyacrylonitrile/polyacrylic acid.

TABLE 2 Summary of the polymer (PAN/PAA)-nanoparticles ratios used for PNFs production

Type of NFs	Ratio (PAN/PAA: nanoparticles)
I. AuNPs (PAN/PAA/AuNPs)	93:7 (v/v)
II. IO (PAN/PAA/IO)	97:3 (v/w)
III. GO (PAN/PAA/GO)	97:3 (v/w)

Abbreviation: AuNP, gold nanoparticles; GO, graphene oxide; IO, iron (III) oxide; PAN/PAA, polyacrylonitrile/polyacrylic acid.

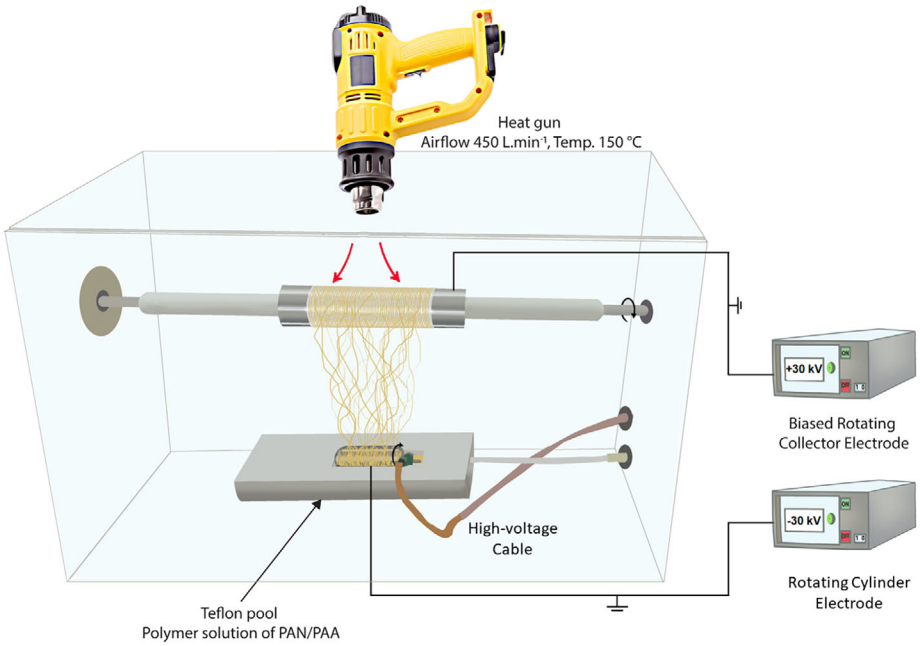

FIGURE 1 A schematic layout of the nozzle-free electrospinning setup [Color figure can be viewed at wileyonlinelibrary.com]

humidity ranging from 30 to 40%. Figure 1 gives a schematic layout of the electrospinning set-up.

2.4 | Stabilization and carbonization

Both stabilization and carbonization processes were performed using a horizontal tube furnace; Pyrolyser model OTX—1,200X (MTI Corporation, USA, Richmond, CA) with a 80 mm internal diameter quartz tube reaction zone having a length of 500 mm, fitted with a Fe—Cr—Al alloy heating element. During the process of temperature, time, heating/cooling rate, and gas atmosphere were carefully controlled. The electrospun PAN/PAA scaffolds (with and without additives) were cut into 6 cm × 3 cm (length × width) mats and clamped on a ceramic tile, with a gap between the clamps of approximately 6 cm. The sample was placed in a boat and inserted into the reaction zone of the tube furnace. The stabilization was performed at 200°C with a heating rate of 10°C min^{-1}, using an air flow rate of 100 mL min^{-1}. The sample was maintained at the final temperature at holding time of 12 hr. Upon completing the stabilization process, the sample was cooled overnight, followed by carbonization performed using the same equipment. The reactor was firstly purged with nitrogen gas for 10–15 min to ensure that all the O_2 was removed. The sample was then ramped to a temperature of 750°C at a heating rate of 10°C min^{-1} using N_2 (flow rate of 100 mL min^{-1}) as the purge gas. Upon reaching the final temperature, the sample was held for 60 min prior to the cooling down period. The changes in weight of the PAN/PAA fibers before and after the processes were recorded using an analytical balance.

2.5 | Morphological and thermochemical characterization

A thermogravimetric analyzer (TGA SDTA 851/1600, Mettler Toledo, USA) was used to observe the thermal stability of the electrospun fibers. Approximately 10 mg of sample was inserted in a 150 μL alumina crucible. The crucible was then inserted in the horizontal furnace and heated to 500 or 900°C at a heating rate of 10°C min^{-1} under purging dry N_2 gas at a rate of 100 mL min^{-1}. To examine the heat flux change of the webs before and after stabilization and carbonization, a differential scanning calorimeter (DSC, PerkinElmer) was used. The sample was heated to 500°C with a heating rate of 10°C min^{-1} under purging N_2 gas.

Attenuated total reflection-Fourier-transform infrared spectroscopy (ATR-FTIR) (Spectrum One, PerkinElmer) was used to explore the changes of the functional groups of the oxidized and carbonized PAN/PAA electrospun fiber mats. The FTIR spectra were recorded between 4,000 and 400 cm^{-1}, averaging three scans. Potassium bromide (KBr) was ground in a mortar to obtain a homogeneous powder was used as the sample matrix and reference material. For sample analysis, CNFs were crushed separately in a mortar and mixed with KBr in a proportion of 50/50 (w/w).

Microscopic observations of the PAN/PAA and carbonized fibers were conducted using a scanning electron microscope (SEM, Hitachi SU3500). Electrospun fibers

were sputter-coated with a thin platinum layer (approximately 10 nm thickness) using a sputter coater (Polaron SC7620, Quorum). To compare the fibers prior/post carbonization, all micrographs were assessed at ×700 magnifications. The fiber size distribution was measured by selecting 100 fibers from the SEM images. The sizes were determined using image processing software ImageJ Version 1.52a[35] and the value was presented as the average. Energy dispersive spectroscopy (EDS) analysis was performed to confirm the presence of nanoparticles in different composite fibers.

2.6 | SPCE characterization and modification

Before the SPCE modification, an electrode pre-treatment was carried out via potential cycling from −2.5 to +2.5 V versus Ag in 0.05 M H_2SO_4 aqueous solution at 0.05 V s^{-1}. This step is crucial to remove any organic contaminants, thus, improving the sensitivity and reproducibility of the readings.[36,37] The various composite fibers with the different nanoparticles were trimmed to have a surface area of about (4 mm^2) and glued onto the working electrode of a treated SPCE using a PELCO® conductive carbon glue. The modified SPCE preparation process is depicted in Figure 2.

2.7 | Electrochemical measurements

The electrochemical characteristics of the modified SPCEs (with the CNFs or PNFs that contain AuNPs, IO, or rGO) were measured by cyclic voltammetry (CV) using a potentiostat controlled by Nova 2.0 software (Autolab PGSTAT204, Metrohm Switzerland). Solutions of $K_3Fe(CN)_6$ and H_2O_2 with different concentrations were prepared by serial dilution of stock solutions in 0.1 M KCl (pH 7.0) and 0.1 M PBS (pH 7.4), respectively. Around 55 μL of the analyte solution was dropped on top of the sensing area's surface, and CV scans were performed as a function of scan rates (0.02, 0.04, 0.06, 0.08, 0.1, and 0.2 Vs^{-1}). The selected voltage windows for $K_3Fe(CN)_6$ and H_2O_2 were − 0.4 to +0.8 V and − 0.2 to +1.2 V, respectively, since their redox peaks appeared within these potential ranges.[38] It should be noted that the background correction at different scan rates is considered at 0 current when performing data analysis.

3 | RESULTS AND DISCUSSION

3.1 | Thermal stabilities of the electrospun PAN/PAA fibers

The optimum stabilization temperature was determined prior to the carbonization. The stabilization process was

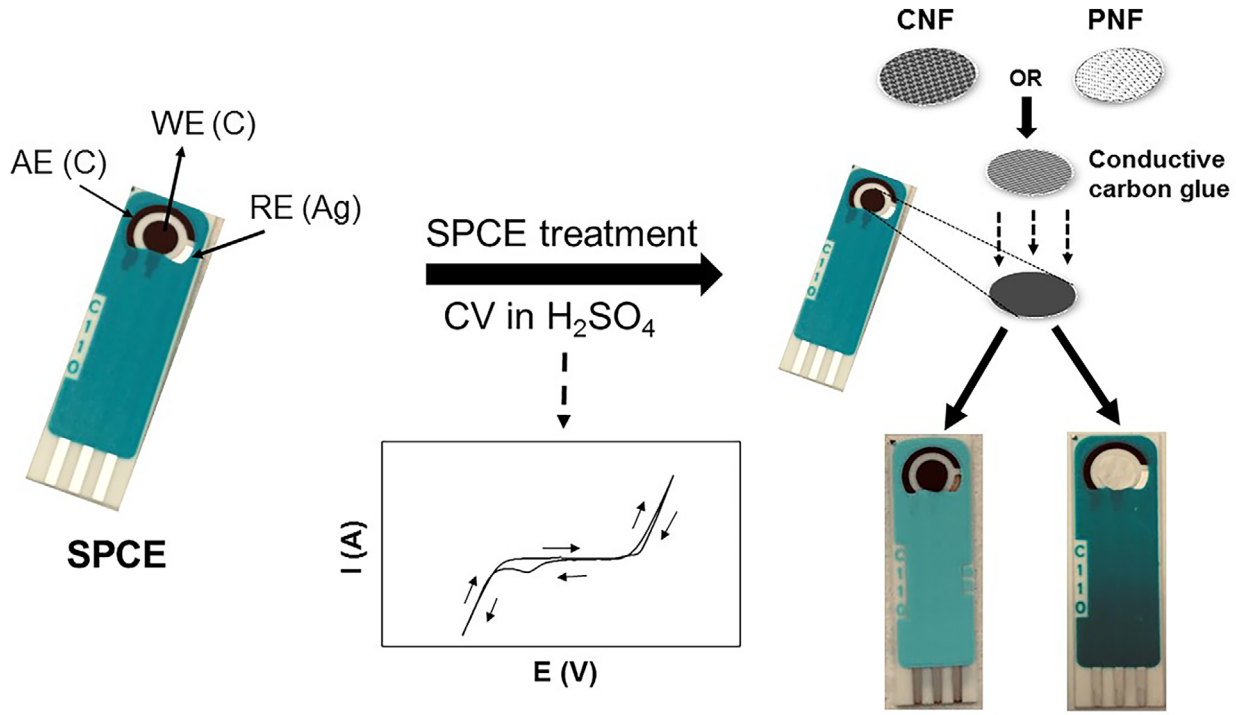

FIGURE 2 Scheme of the preparation of screen-printed carbon electrode (SPCE) modified electrode. SPCE was treated via potential cycling in 0.05 M H_2SO_4. Nanofibers were trimmed and glued onto the working electrode of the treated SPCE using a conductive carbon glue [Color figure can be viewed at wileyonlinelibrary.com]

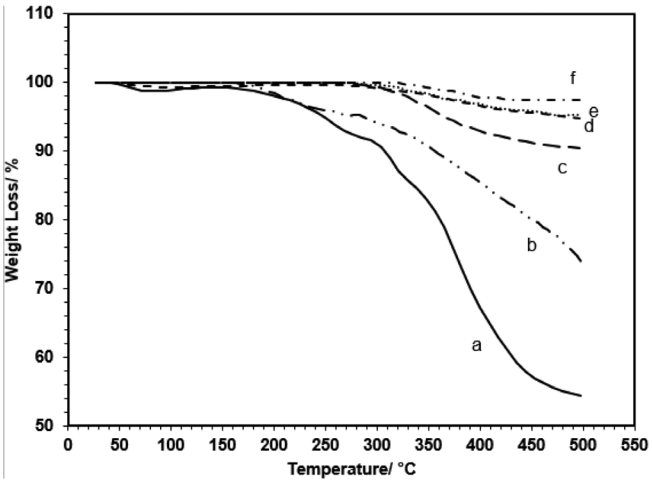

FIGURE 3 Thermogravimetric analyzer (TGA) thermograms measured in N_2 for polyacrylonitrile/polyacrylic acid (PAN/PAA) precursor nanofibers (PNFs) without additives (a), the PNFs without additives stabilized for 12 hr (b), the carbonized PAN/PAA nanofibers with gold nanoparticles (AuNPs) (c), the carbonized PAN/PAA nanofibers with iron (III) oxide (IO) (d), the carbonized PAN/PAA nanofibers without additives (e), and the carbonized PAN/PAA nanofibers with graphene oxide (GO) (f)

performed at a controlled temperature of 200°C by using 12 hr of stabilization time. The shrinkage percentage was controlled between 10.4 and 12.5% (refer to Figures S1 and S2). The long stabilization time was used to ensure that the PAN/PAA fibers were cyclized.[23] The long stabilization time not only increased the number of ladder polymers in stabilized nanofibers but also improved the physical properties of the resulting carbon nanofibers. Figure 3 shows the thermal stability of the PNFs, and the stabilized carbonized NFs with and without additives. There was a slight weight loss of about 3–5% near 100°C that may be due to the removal of moisture from the non-carbonized precursor NFs (Figure 3a. The PAN/PAA PNF material remains stable up to the temperature of 200°C. The untreated sample lost weight over a narrow temperature range in comparison to the stabilized sample due to greater formation of ladder-like structures related to oxidation-based cross-linking.[39] The large secondary weight loss seen beyond this temperature was due to the removal of the chemical groups formed on the fiber surfaces. The unchanged sample weight between 100 and 200°C indicates that no chemical reaction occurred and can be ascribed by the cyclization process.[24] In the case of the stabilized nanofibers, it was found that the sample is stable until approximately 200°C, due to the effect of stabilization under oxygen condition, which is related to the cyclization of nitrile groups, cross-linking of the chain molecules and dehydrogenation promote the formation of the ladder structure from the linear molecule.[39] The ladder structure polymers are more stable in heat than linear polymers as the special structure prevents them from melting at higher temperatures.[40] The heat-treated (stabilized and carbonized) nanofibers were thermally stable up to 500°C. Such thermal behavior was typically seen in PAN-based carbon fibers.[21,24] The presence of rGO showed the highest thermal stability with the minimal weight loss of about 2.5 wt%. Improvement of nanocomposite thermal stability was due to the formation of carbonaceous protective layer that led to a lower rate of heat transfer as well as mass loss of the polymer.[41] In addition, the incorporation of rGO would constrain the mobility of the polymeric chains via physical or chemical interfacial bonds, resulted in prominent thermal stability of the nanofiber.[21,42]

3.2 | ATR-FTIR analysis

FTIR analysis was performed to identify any changes to the chemical composition of the PAN/PAA NFs before and after carbonization. There were distinguishable changes in the characteristic absorption peaks of PAN and PAA at several locations of the spectrum. Most of the strong and sharp peaks in the precursor web disappeared after carbonization, as shown in Figure 4. Notably, the strong absorption peak located between 2,260 and 2,200 cm^{-1} can be attributed to the characteristic nitrile (—C≡N) groups of PAN. The apparent decrease at the peak intensity at 2,243 cm^{-1} could be explained by the reaction of nitrile groups during the cyclization process to form conjugated C═N groups. Absorption peaks in the region between 1,300–1,800 cm^{-1} could be attributed to the presence of water molecules.[40] Weak absorption peaks at around 1,600 cm^{-1} present in the CNFs specimens can be assigned to a combined effect of C═N, C═C, N—H groups,[39] and the peak near 1,400 cm^{-1} to C—H bonding.[26] The disappearance of the peaks at around 800 and 3,000 cm^{-1} in the CNFs samples shows that the carbonization process has successfully eliminated all the ═C—H, and C—H bonds present, indicating that the cross-linking of the chain molecules and dehydrogenation were complete.[23] The DSC thermograms of the PAN/PAA PNFs, the stabilized, and the carbonized nanofibers further confirmed the completion of cyclization during the carbonization process (see Figure S3).

3.3 | Electrospun fiber morphology

The carbonization process can lead to increased mechanical strength.[22] A carbon content of 90% can be expected in the PAN fibers after carbonization.[43] Figure 5 shows a series of SEM micrographs of PAN/PAA PNFs and

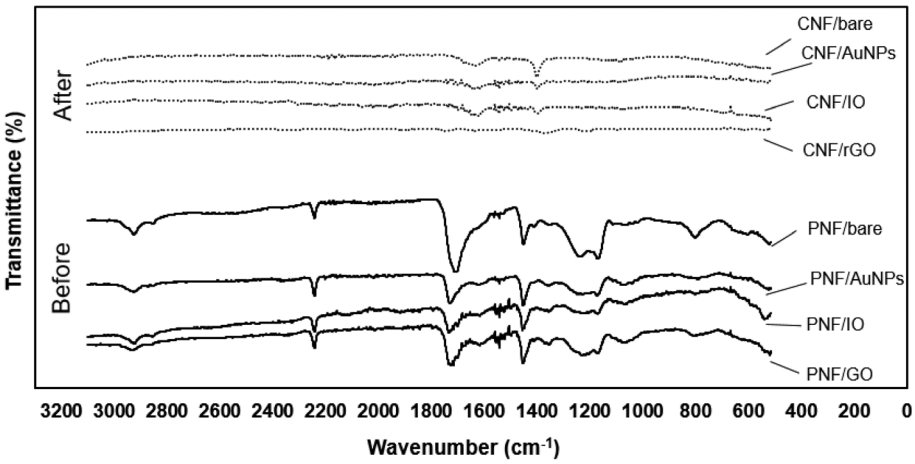

FIGURE 4 Fourier-transform infrared spectroscopy (FTIR) spectra of the polyacrylonitrile/polyacrylic acid (PAN/PAA) nanofibers with nanoparticles of gold, iron oxide, graphene oxide (GO)/reduced graphene oxide (rGO) and control (bare) before (solid line: precursor nanofibers [PNFs]) and after carbonization (dotted line: carbon nanofibers [CNFs])

CNFs, which illustrate the effect of carbonization on the morphological appearance of the fibers. The inset shows the distribution of the average diameter of the filaments in the fiber examined using an image analyzer software. The respective fiber diameters are provided in Table 3 below, while the individual size distribution can be found in Table S1. The fibers maintained their shape after carbonization with reduced fiber diameters. The nanoparticles of AuNPs, IO, or GO/rGO were homogenously dispersed within the electrospun fiber matrix. Energy dispersive spectroscopy (EDS) analysis during electron microscopy confirms the presence of AuNPs, IO, or rGO (see Figure S4, S5, and S6). The rGO appeared to be semi-transparent (see Figure 5d2) as it is electron transparent and stable in the electron beam.[44] The average diameter of the bare PNFs was 708 ± 265 nm. Thicker fibers were obtained when PAN/PAA was electrospun with nanoparticles, yielding 1,418 ± 390 nm, 1,129 ± 259 nm, 961 ± 207 nm for nanofiber composites containing AuNPs, IO, and rGO, respectively. This finding is in agreement with Kim et al. in which a 50 nm increase of fiber diameter was observed after addition of AuNPs to poly (ethylene oxide).[45] Following carbonization, the fiber diameter of the bare CNFs was reduced to 455 ± 177 nm, while the NFs containing AuNPs, IO, or rGO were also reduced to 747 ± 189, 1,010 ± 345, and 428 ± 93 nm, respectively.

The reduction in fiber diameter is due to the elimination of the volatile compounds and shrinkage, attributable to the entropic and chemical shrinkage.[40] The chemical shrinkage is caused by the formation of dense structures after chemical reactions, while the entropic shrinkage is caused mainly by the retraction of stretched polymer chains, which is independent of the heating rate.[46] The fiber diameter distribution obtained in this study was considered appropriate to prepare the carbon NFs, while taking into account the significant reduction of the diameter during carbonization and of the uniformity of the fibrous meshes after heat-treatment.

3.4 | Electrochemical performance of SPCE with nanofiber electrodes

3.4.1 | Effect of the carbon glue on the redox reaction

The effect of the carbon glue on the charge transferability of the analytes on the SPCE was assessed by comparing the electrochemical performances of the SPCE without modification, and that of the SPCE with a layer of carbon glue via CV measurements in 2 mM $K_3Fe(CN)_6$ or 5 mM H_2O_2 solutions. Figure 6a indicates that the SPCE with or without carbon glue shows reversible redox reactions towards $K_3Fe(CN)_6$ at ~0.2 and 0.03 V, respectively. However, SPCE with carbon glue demonstrated less pronounced oxidation and reduction peaks. The background-subtracted oxidation peak signal at ~0.2 V of the SPCE with glue is approximately 4.2 times less than that of the SPCE. In the case for H_2O_2 (Figure 6b), the SPCE with the carbon glue exhibited a much lower oxidation current of an irreversible redox reaction towards H_2O_2. Since there is no apparent oxidation peak, the H_2O_2 responses of the modified SPCEs were compared with the oxidation currents at a potential of 1.1 V. The background-corrected signal at 1.1 V for the SPCE with carbon glue was found to be approximately 1.8 times lower than that of the SPCE, indicating that the SPCE presented a decreased active surface area, electronic mobility, and electron transfer rate as a result of the additional layer of carbon glue. A small-signal peak (~1.0 V) of the oxidation current was observed in the SPCE containing carbon glue from a potential of 0.4 V. This enhancement was also seen at the same potential (~1.0 V) in other CV measurements using modified SPCEs (Figure S7). This enhancement could be attributed to the reaction between H_2O_2 and other chemicals present in the carbon glue, which were ignored in the data interpretations.

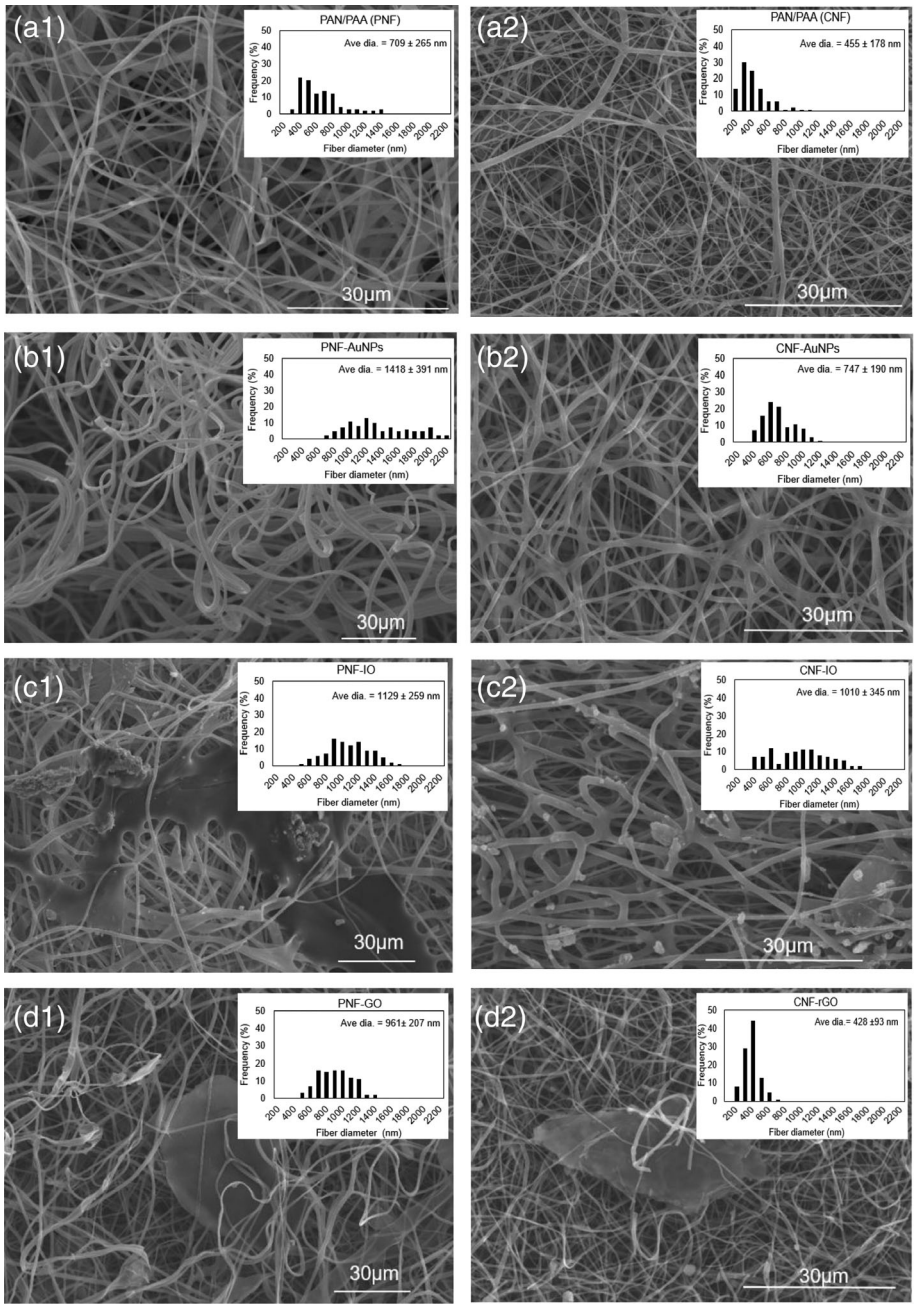

FIGURE 5 Scanning electron microscope (SEM) images of precursor nanofibers (PNFs) (a1–d1) and carbonized nanofibers (CNFs) (a2–d2). The fibers maintained their shape after carbonization with reduced fiber diameter. Nanoparticles of gold, iron oxide or graphene oxide (GO)/reduced graphene oxide (rGO) were homogenously dispersed within the electrospun fibers matrix

TABLE 3 Average diameter of PNFs and CNFs decorated with different particles

Type of nanoparticles	PNF (nm)	CNF (nm)
Bare	709 ± 265	455 ± 178
AuNPs	1,418 ± 391	747 ± 190
IO	1,129 ± 259	1,010 ± 345
GO/rGO	961 ± 207	428 ± 93

Abbreviation: AuNP, gold nanoparticles; CNF, carbon nanofibers; GO, graphene oxide; IO, iron (III) oxide; PNF, precursor nanofibers.

3.4.2 | Effect of the carbon glue on the electroactive surface area

The effect of the carbon glue used to attach the CNF or PNF composites to the SPCEs on the electroactivity of the transducer matrix was evaluated by estimating the electroactive surface area (ESA) of the SPCE and modified SPCE by the Randles-Sevcik equation[47],

$$I_p = 2.69 \times 10^5 \times n^{3/2} \times A \times C \times (D \times \mathrm{v})^{1/2}$$

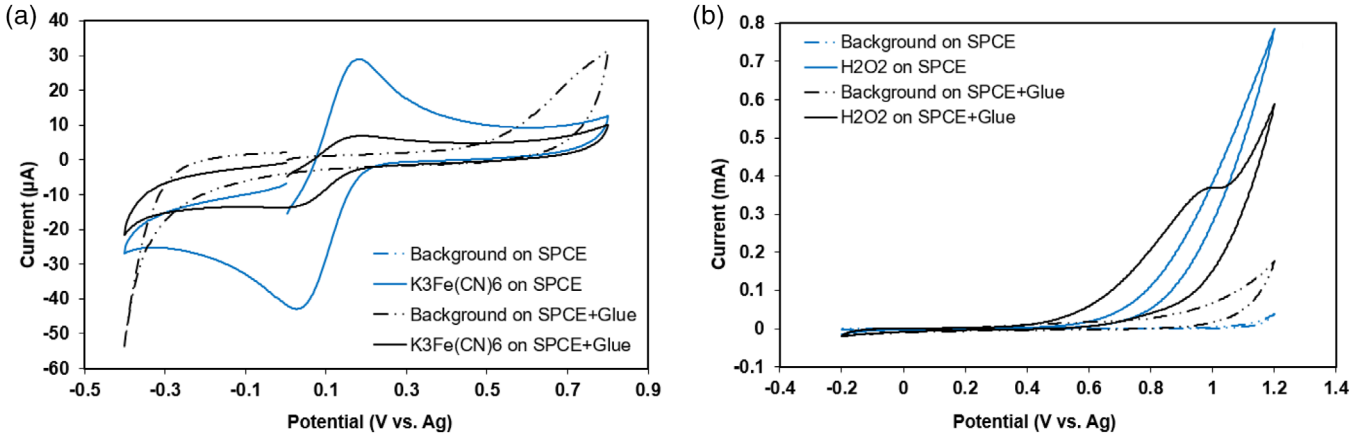

FIGURE 6 Cyclic voltammograms of screen-printed carbon electrode (SPCE) and SPCE with carbon glue in (a) 2 mM $K_3Fe(CN)_6$ (background was 0.1 M KCl) and (b) 5 mM H_2O_2 (background was 0.1 M phosphate buffer saline (PBS) (pH 7.4)) and the scan rate was 0.1 V s^{-1}. Addition of carbon glue decreased the oxidation signals for $K_3Fe(CN)_6$ and H_2O_2 [Color figure can be viewed at wileyonlinelibrary.com]

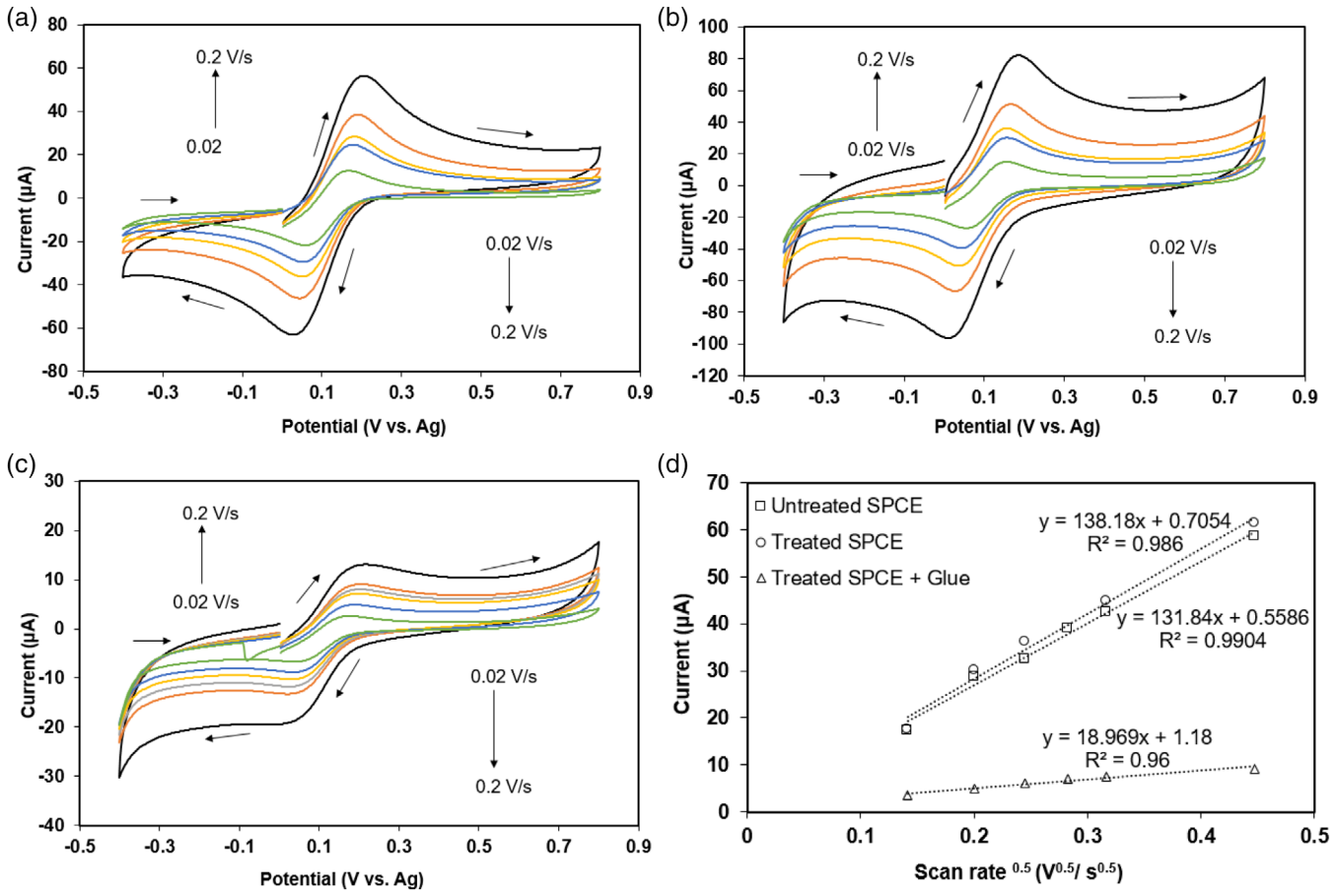

FIGURE 7 Cyclic voltammograms related to the untreated screen-printed carbon electrode (SPCE) (a), treated SPCE (b), treated SPCE with conductive carbon glue (c), under different scan rates (0.02, 0.04, 0.06, 0.08, 0.1 and 0.2 V s^{-1}) in 0.1 M KCl + 2 mM $Fe(CN)_6^{3-/4-}$, and the relationship between the oxidation current peaks of the redox species at the electrodes and the square root of corresponding scan rates (d) [Color figure can be viewed at wileyonlinelibrary.com]

where I_p is the peak current [A], n is the number of electron transfers per reaction [1 for $Fe^{3+/4+}$], A is the electrochemical surface area [$= \pi\ (0.2)^2 = 0.126\ cm^2$], C is the concentration (mol cm^{-3}), D is the diffusion constant [$7.6 \times 10^{-6}\ cm^2\ s^{-1}$] and v is the scan rate [$V\ s^{-1}$].

The SPCE was treated with sulfuric acid to remove its organic contaminants and to improve the surface electroactivity before applying the carbon glue. The CV measurements were then performed using 2 mM $Fe(CN)_6^{3-/4-}$ solutions to compare the electrochemical performances of the NF electrodes. As seen in Figure 7, there was a linear trend between the square root of the scan rate and the anodic current peak as a consequence of a reversible reaction mechanism limited by diffusion[48] for the treated and untreated SPCE, as well as the treated SPCE with carbon glue. The electroactive area of the untreated electrode, with a geometric area of 0.126 cm^2, was estimated as 0.0889 cm^2 before the treatment. The treated SPCE had a 5% increase in electroactive area (ESA = 0.0932 cm^2); while the treated SPCE with carbon glue had a reduction of 85% (ESA = 0.0128 cm^2) of its electroactive area. This observation indicates that the carbon glue greatly hinders the interfacial charge transfer.

3.5 | Scan rate dependent study

The dynamic behavior of the modified SPCE was assessed through CV responses in 5 mM H_2O_2 and 2 mM $K_3Fe(CN)_6$ at different scan rates ranging from 0.02 to 0.2 $V\ s^{-1}$. Figure 8 shows that the redox current response for $K_3Fe(CN)_6$ is noticeably dependent on the scan rate of the SPCEs modified with PNFs (Figure 8a–d) and CNFs (Figure 8e–h). Besides, the current, as well as the peak potential for $K_3Fe(CN)_6$ redox peaks, are monotonically increased with increasing scan rates. Thus, redox reactions of $K_3Fe(CN)_6$ on the NF electrode are relatively slow and considerably limited by the scan rate. To further identify the reaction mechanisms for the modified SPCEs, the oxidation peaks for the $K_3Fe(CN)_6$ was plotted versus the scan rate, as illustrated in Figure 8i and j. The oxidation peak amplitude for $K_3Fe(CN)_6$ increases linearly with the square root of the scan rate. The results indicate that the reactions of $K_3Fe(CN)_6$ on the nanofiber electrode follow the typical semi-infinite diffusion mechanism.[38] In the case of the SPCE modified with bare PNFs or CNFs, the electron transfer kinetics were rather slow during the redox reactions of $[Fe(CN)_6]^{3-/4-}$ with low anodic current density. However, the SPCE modified with CNFs decorated with nanoparticles show higher oxidation peaks than that of the equivalent PNF composite, demonstrating significantly improved responses towards the $K_3Fe(CN)_6$ solutions. The SPCE modified with CNF-rGO showed the most prominent increment, indicating excellent electron conduction between the surface of the electrode and the electrolyte solution. Additionally, an increasing peak separation with the increased scan rates for all the PNF and CNF electrodes (see Figure S7), showing a quasi-reversible process[49]. This evidenced that the PNF and CNF composite electrodes are stable towards the detection of $K_3Fe(CN)_6$. The higher capacitive behavior observed in the CNF composite electrodes than the corresponding PNF electrodes is due to the carbonization process that resulted in an increased surface area and carbon content of the CNF electrodes.

In contrast, Figure 9 shows that the current response for H_2O_2 varies slowly between scan rate variations, which indicates that the oxidation of H_2O_2 on the nanofiber electrode is quite fast so that a similar reaction rate is obtained at a different activation rate. A small peak at the oxidation current (potential ~1.0 V) was apparent in all the SPCE modified with PNFs (Figure 9a–d), as a result of the presence of the carbon glue. The same peak at the oxidation current was less prominent in the modified SPCE with the CNFs. Figure 9i,j shows the oxidation currents at the potential of 1.2 V versus the scan rate. The oxidation peak amplitude for H_2O_2 increases linearly with the square root of the scan rate, indicating that the reactions of H_2O_2 on the nanofiber electrode follow the semi-infinite diffusion mechanism.[38] The SPCE modified with CNFs decorated with nanoparticles shows higher oxidation peaks than that of the equivalent PNF composites, indicating significantly improved responses towards the H_2O_2 solutions. The SPCE modified with CNF-rGO showed the greatest current density among the various modified electrode.

The effect of the different CNF and PNF composites on the electroactivity of the transducer was further evaluated by quantifying the electroactive surface area of the SPCEs before and after modification. The electroactive surface area of the SPCE with carbon glue only is considered as a baseline for the comparison of the electrochemical responses among the different CNF and PNF composites electrodes (Figure 10). The CNF composites demonstrated higher electroactive area than the PNF composites, while the bare CNFs and PNFs did not present any significant difference. The CNF composites performed better than the equivalent PNFs composites due to the formation of a ladder structure through the process of nitrile polymerization following the carbonization step. This structure offers the advantages of good electrochemical activity and conductivity.[30] CNFs containing rGO

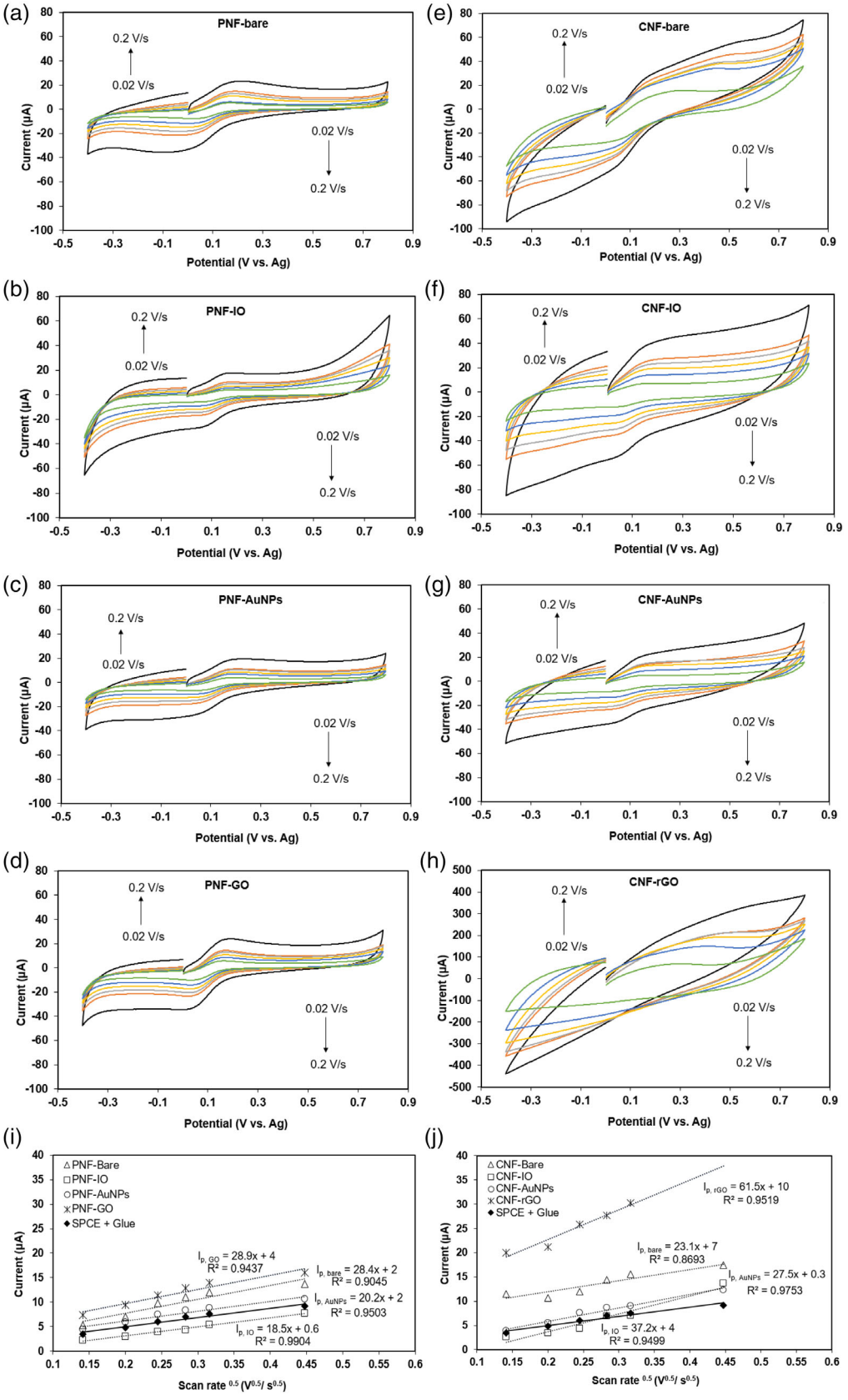

FIGURE 8 CV responses of the precursor nanofibers (PNFs) (a-d) and carbonized nanofibers (e-h) composites towards 2 mM $K_3Fe(CN)_6$ (a,e: bare, b,f: iron oxide, c,g: gold nanoparticles, d: GO, h: rGO). Oxidation current peaks for (i) PNFs composites and (j) carbonized nanofibers composites towards $K_3Fe(CN)_6$ vs. the square root of scan rate [Color figure can be viewed at wileyonlinelibrary.com]

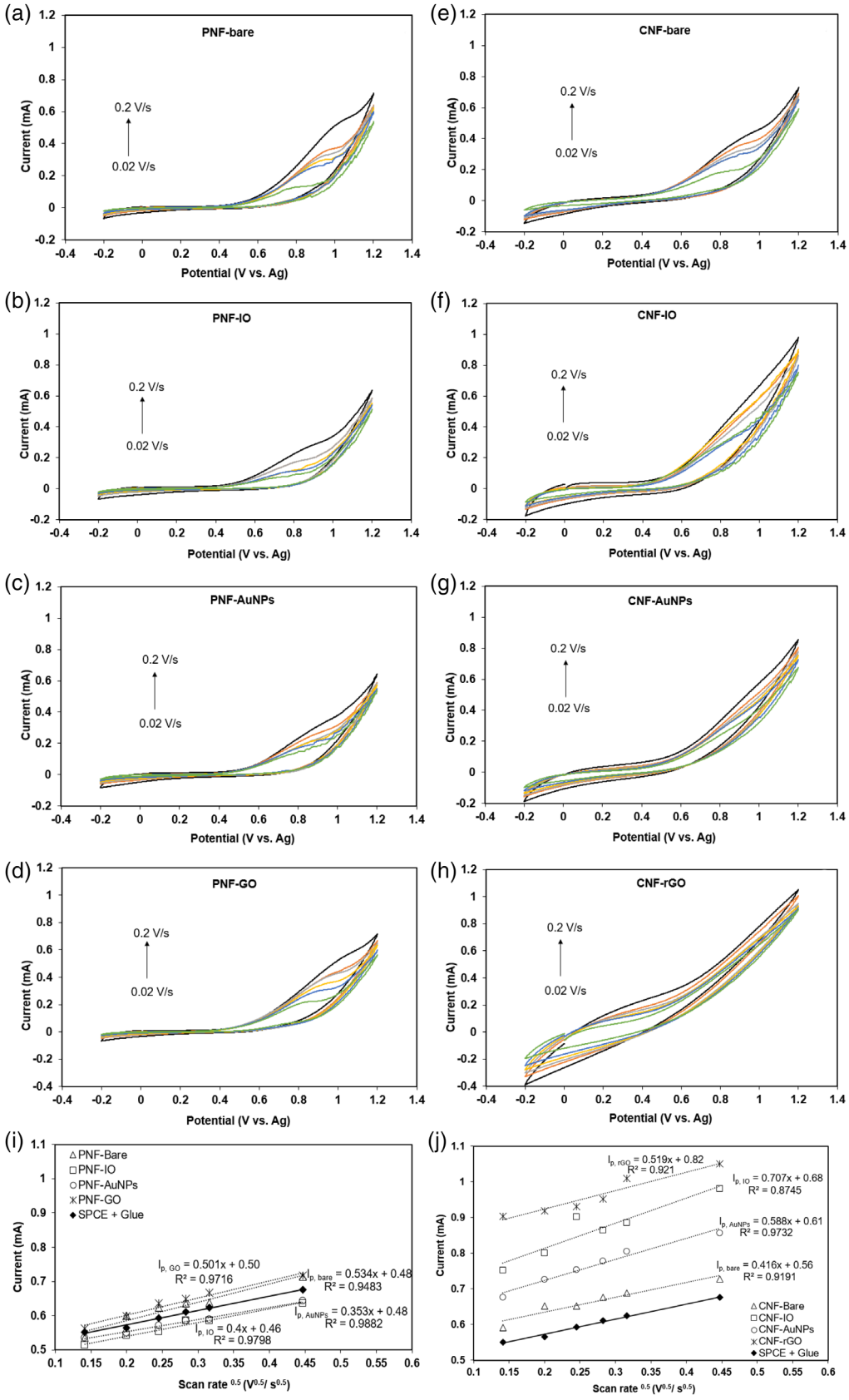

FIGURE 9 Cyclic voltammetry (CV) responses of the precursor nanofibers (PNFs) (a–d) and carbonized nanofibers (e–h) composites towards 2 mM H_2O_2 (a,e, bare, b,f, iron oxide, c,g, gold nanoparticles, d, GO, h, rGO). Oxidation currents for (i) PNFs composites and (j) carbonized nanofibers composites towards H_2O_2 at 1.2 V vs. the square root of scan rate [Color figure can be viewed at wileyonlinelibrary.com]

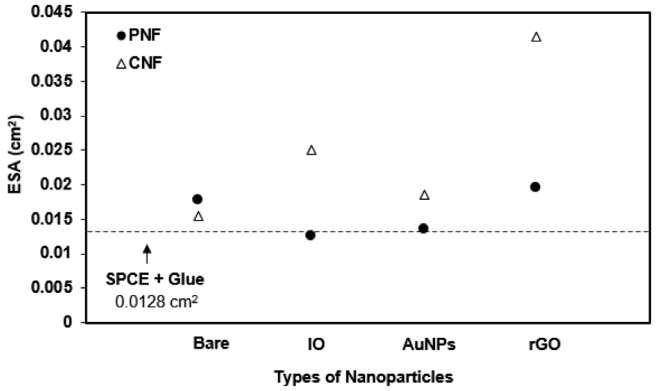

FIGURE 10 Electroactive surface area (ESA) of the screen-printed carbon electrode (SPCEs) modified by carbon nanofibers (CNFs) and precursor nanofibers (PNFs) decorated with different nanoparticles

showed the highest improved performance of 2.13 times, followed by CNF-IO (2 times greater) and CNF-AuNPs (1.37 times greater) than that of the non-carbonized counterparts. This indicates that the nanoparticle inclusion can enhance the active surface area of composite electrodes effectively. The SPCE modified with CNF-rGO exhibited the most significantly enhanced response towards $K_3Fe(CN)_6$ and H_2O_2 solutions due to the increased reactive surface area and extraordinary electrical conductivity by the graphene incorporation.[24,50]

The key factors contributing to the electrochemical properties of an electrode containing nanoparticles are the sizes and concentrations of the nanoparticles. Even though CNF-rGO exhibited the highest response increment among the types of nanoparticles examined in this study, the effect of nanoparticle content in the nanofiber composite is required to obtain more significant conclusions. However, a comparison with the previous studies has shown that the nanoparticle concentrations of rGO and IO used in the present work are not far from the optimum concentrations, which are 10 [38] and 4 wt%,[51] respectively. Low performance of NF-AuNPs found in this study was attributed to the low concentration of the AuNPs (nano-molar) in the NFs, compared to other electrospun nanofiber electrodes that used AuNPs in the range of micro- or milli-molar.[30,52] The significantly improved responses as seen in the CNF composite electrodes are due to the higher surface area of CNFs electrodes that can absorb relatively more target molecules compared to PNF electrodes. In addition, all the CNF composite electrodes have good electron transfer ability, compared to PNF composite electrodes as a result of higher carbon content. The loaded nanoparticles can form a sparser conductive network inside the nanocomposite, which can enhance the electrical conductivity of the CNFs.[24,53,54] This effect is most prominent in CNF-rGO that showed the highest ESA value, indicative of the superior electrochemical activity and conductivity. Thus, it is possible to infer that carbonized nanofibers containing rGO are a suitable material in fabricating low cost, high-performance sensor by electrospinning technology.

4 | CONCLUSIONS

Electrospun PAN/PAA NFs were produced via the electrospinning process and used as a precursor for producing PAN-derived carbon NFs. TGA and DSC results confirmed the successful stabilization and carbonization of the PAN NFs. SEM images revealed that the addition of nanoparticles changes the fiber morphology by increasing the fiber diameters. Fibers maintained their shape post-carbonization with a reduced diameter being apparent with the nanoparticles of AuNPs, IO, or rGO homogeneously dispersed within the electrospun fiber-matrix. SPCEs modified with CNF or PNF composites were successfully developed for the electrochemical detection of H_2O_2 and $(Fe(CN)_6^{3-/4-})$ redox couples. The influence of the carbon glue was quantified, where it was observed that the ESA of the SPCE was greatly reduced post-application of the glue. The incorporation of nanoparticles into the nanofiber presented increased electroactive area in the CNFs electrode with CNF-rGO (~2.13 times), CNF-IO (~2 times) and CNF-AuNPs (~1.37 times) greater than those of PNFs equivalents. The modified SPCE with CNF composites showed enhanced responses towards $K_3Fe(CN)_6$ and H_2O_2 solutions, when compared with the modified SPCE with PNF composites. The CNF-rGO exhibited the most significantly improved response, followed by CNF-IO and CNF-AuNPs. Finally, despite suffering from the inhibitive effect of carbon glue as the charge transfer barrier, this work provides a simple strategy of utilizing electrospun produced fibers (CNFs sheet) straightforwardly without complicated fabrication steps involving advanced machines. This work demonstrates a promising tool for developing sensing platforms for electrochemical detection.

ACKNOWLEDGMENTS

The authors would like to acknowledge the School of Engineering from the University of Edinburgh for the funding through the McCann Prize (grant number: 100-IRMI/INT 16/6/2 [010/2017]). The authors would further wish to thank the Universiti Teknologi MARA for the support and some of scientific equipment used

in this study. The authors also would like to thank Ignacio Tudela, Francisco Javier Diaz Sanchez, and Andreas Tsiamis for their help with the electrochemical analysis. Finally, the authors would also like to thank Fergus Dingwall, Daniel Wilhelm, Ahmad Deedat Shafiei, and Noor Hafizah Tahal@Tahar for the laboratory assistance.

CONFLICT OF INTEREST

The authors declare no conflicts of interest.

ORCID

Huey Ling Tan https://orcid.org/0000-0001-8580-8858

REFERENCES

[1] S. Thenmozhi, N. Dharmaraj, K. Kadirvelu, H. Yong, *Mater. Sci. Eng. B* **2017**, *217*, 36.
[2] C. Chen, Y. Tang, B. Vlahovic, F. Yan, *Nanoscale Res. Lett.* **2017**, *12*, 451.
[3] Z.-M. Huang, Y.-Z. Zhang, M. Kotaki, S. Ramakrishna, *Compos. Sci. Technol.* **2003**, *63*, 2223.
[4] A. E. Palmqvist, *Curr. Opin. Colloid Interface Sci.* **2003**, *8*, 145.
[5] Z. D. Feng, S. Li, H. Li, J. Zhai, Y. Song, L. Jiang, *Angew Chem Int Ed* **2002**, *41*, 1221.
[6] G. M. Whitesides, B. Grzybowski, *Science* **2002**, *295*, 2418.
[7] S. G. Leonardi et al., *Nanotechnology* **2016**, *27*, 075502.
[8] *Appl. Surf. Sci.* **2015**, *353*, 594.
[9] S. V. Ebadi, A. Fakhrali, S. O. Ranaei-Siadat, A. A. Gharehaghaji, S. Mazinani, M. Dinari, J. Harati, *RSC Adv.* **2015**, *5*, 42572.
[10] Y. Liu, M. Park, B. Ding, J. Kim, M. el-Newehy, S. S. Al-Deyab, H. Y. Kim, *Fibers Polym.* **2015**, *16*, 629.
[11] T. Homma, M. Kondo, T. Kuwahara, M. Shimomura, *Eur. Polym. J.* **2015**, *62*, 139.
[12] B. Ding, M. Yamazaki, S. Shiratori, *Sensors Actuators B Chem.* **2005**, *106*, 477.
[13] H. Niu, T. Lin, *J. Nanomater* **2012**, *2012*, 725950.
[14] F. Miao, C. Shao, X. Li, K. Wang, Y. Liu, *J. Mater. Chem. A* **2016**, *4*, 4180.
[15] H. Niu, X. Wang, T. Lin, *Nanofibers: Production, Properties and Functional Application*, IntechOpen, London **2011**, p. 17.
[16] E. Ismar et al., *J. Appl. Polym. Sci.* **2018**, *135*, 4180.
[17] W. K. Chee, H. N. Lim, Z. Zainal, I. Harrison, N. M. Huang, Y. Andou, K. F. Chong, A. Pandikumar, *RSC Adv.* **2017**, *7*, 12033.
[18] Q. Li, Z. Hu, Z. Liu, Y. Zhao, M. Li, J. Meng, X. Tian, X. Xu, L. Mai, *Chem. - A Eur. J.* **2018**, *24*, 18307.
[19] H. Wang, X. Zhang, Y. Zhang, et al., *J. Appl. Polym. Sci.* **2016**, *133*, 43914.
[20] S.-J. Park, *Carbon Fibers*, Vol. 210, Springer, Berlin **2015**.
[21] S. Faraji, M. F. Yardim, D. S. Can, A. S. Sarac, *J. Appl. Polym. Sci.* **2017**, *134*, 1.
[22] Z. Wangxi, L. Jie, W. Gang, *Carbon N. Y.* **2003**, *41*, 2805.
[23] H.-I. Joh, S. Lee, J. Kim, J. Kim, B.-C. Ku, *Adv. Chem. Eng. Sci.* **2012**, *02*, 275.
[24] I. Gergin, E. Ismar, A. S. Sarac, *Beilstein J. Nanotechnol.* **2017**, *8*, 1616.
[25] D. D. Edie, R. J. Diefendorf, Chapter 2 - carbon fiber manufacturing. in *Carbon–carbon materials and composites* (Eds: J. D. Buckley, D. D. Edie), William Andrew Publishing, Oxford **1993**, p. 19.
[26] S. N. Arshad, M. Naraghi, I. Chasiotis, *Carbon N. Y.* **2011**, *49*, 1710.
[27] I. Ismail, N. F. A. Bakar, H. L. Tan, N. Ideris, Z. H. M. Zain, N. Radacsi, *Mater. Today Proc.* **2019**, *17*, 574.
[28] S. S. Abe Jyunichiro, T. Keisuke, K. Koki, K. Yuta, *ACS Appl. Nano Mater.* **2018**, *1*, 2982.
[29] C. Liu, G. Shi, G. Wang, P. Mishra, S. Jia, X. Jiang, P. Zhang, Y. Dong, Z. Wang, *RSC Adv.* **2019**, *9*, 6898.
[30] B. Bera, M. Das Sarkar, *IOSR J. Appl. Phys.* **2017**, *09*, 05.
[31] S. Yarova, D. Jones, F. Jaouen, S. Cavaliere, *Surfaces* **2019**, *2*, 159.
[32] Z. A. Alothman, *Materials (Basel).* **2012**, *5*, 2874.
[33] A. S. Levitt, M. Alhabeb, C. B. Hatter, A. Sarycheva, G. Dion, Y. Gogotsi, *J. Mater. Chem. A* **2019**, *7*, 269.
[34] D. C. Marcano, D. V. Kosynkin, J. M. Berlin, A. Sinitskii, Z. Sun, A. Slesarev, L. B. Alemany, W. Lu, J. M. Tour, *ACS Nano* **2010**, *4*, 4806.
[35] C. A. Schneider, W. S. Rasband, K. W. Eliceiri, *Nat. Methods* **2012**, *9*, 671.
[36] Pine Research Instrumentation, *Screen-Printed Electrode Information*, Vol. 10036, Pine Research Instrumentation, Durham **2016**, p. 1.
[37] L. G. Mohtar et al., *Microchem. J.* **2019**, *144*, 13.
[38] C. Karuwan, A. Wisitsoraat, D. Phokharatkul, C. Sriprachuabwong, T. Lomas, D. Nacapricha, A. Tuantranont, *RSC Adv.* **2013**, *3*, 25792.
[39] S. Dalton, F. Heatley, P. M. Budd, *Polymer (Guildf).* **1999**, *40*, 5531.
[40] J. Meinl, M. Kirsten, C. Cherif, A. Michaelis, *Am. J. Anal. Chem.* **2016**, *07*, 282.
[41] M. Ajorloo, M. Fasihi, M. Ohshima, K. Taki, *Mater. Des.* **2019**, *181*, 108068.
[42] F. Yavari, H. R. Fard, K. Pashayi, M. A. Rafiee, A. Zamiri, Z. Yu, R. Ozisik, T. Borca-Tasciuc, N. Koratkar, *J. Phys. Chem. C* **2011**, *115*, 8753.
[43] E. Zussman, X. Chen, W. Ding, L. Calabri, D. A. Dikin, J. P. Quintana, R. S. Ruoff, *Carbon N. Y.* **2005**, *43*, 2175.
[44] N. R. Wilson, P. A. Pandey, R. Beanland, R. J. Young, I. A. Kinloch, L. Gong, Z. Liu, K. Suenaga, J. P. Rourke, S. J. York, J. Sloan, *ACS Nano* **2009**, *3*, 2547.
[45] G. Kim, A. Wutzler, H.-J. Radusch, et al., *Chem Mater* **2005**, *17*, 4949.
[46] I. M. Alarifi, W. S. Khan, R. Asmatulu, *PLoS One* **2018**, *13*, 1.
[47] R. A. Dorledo de Faria, H. Iden, L. G. D. Heneine, T. Matencio, Y. Messaddeq, *Sensors* **2019**, *19*, 1686.
[48] A. Suea-Ngam, P. Rattanarat, K. Wongravee, O. Chailapakul, M. Srisa-Art, *Talanta* **2016**, *158*, 134.
[49] P. K. Lee, P. M. Woi, *J. Electroanal. Chem.* **2019**, *837*, 67.
[50] H. I. Joh, H. K. Song, C. H. Lee, J. M. Yun, S. M. Jo, S. Lee, S. I. Na, A. T. Chien, S. Kumar, *Carbon N. Y.* **2014**, *70*, 308.
[51] M. M. Vinay, Y. A. Nayaka, *J. Sci. Adv. Mater. Devices* **2019**, *4*, 442.
[52] F. L. Migliorini, K. B. R. Teodoro, V. P. Scagion, D. M. dos Santos, F. J. Fonseca, L. H. C. Mattoso, D. S. Correa, *Surfaces* **2019**, *2*, 432.

[53] L. Duan, D. R. D'Hooge, M. Spoerk, P. Cornillie, L. Cardon, *ACS Appl. Mater. Interfaces* **2018**, *10*, 22678.
[54] B. Hu, N. Hu, Y. Cai, W. Yuan, C. Yan, Y. Cai, M. Furukawa, M. Matsushita, *Smart Mater. Struct.* **2013**, *22*, 045008.

SUPPORTING INFORMATION

Additional supporting information may be found online in the Supporting Information section at the end of this article.

How to cite this article: Tan HL, Sanira Putri MK, Idris SS, et al. High-throughput fabrication of carbonized electrospun polyacrylonitrile/poly(acrylic acid) nanofibers with additives for enhanced electrochemical sensing. *J Appl Polym Sci*. 2020;e49341. https://doi.org/10.1002/app.49341